Article:
Jeannin, M, Bonazzi, T, Gacemi, D et al. (6 more authors) (2020) Absorption Engineering in an Ultrasubwavelength Quantum System. Nano Letters, 20 (6). pp. 4430-4436. ISSN 1530-6984

https://doi.org/10.1021/acs.nanolett.0c01217

Supporting Information for:

Absorption engineering in an ultra-subwavelength quantum system

Mathieu Jeannin,[1] Thomas Bonazzi,[1] Djamal Gacemi,[1] Angela Vasanelli,[1] Lianhe Li,[2] Alexander Giles Davies,[2] Edmund Linfield,[2] Carlo Sirtori[1] and Yanko Todorov[1],*

[1]Laboratoire de Physique de l'Ecole Normale Supérieure, ENS, Paris Sciences et Lettres, CNRS, Université de Paris, 24 Rue Lhomond, 75005 Paris, France

[2]School of Electronics and Electrical Engineering, University of Leeds, LS2 9JT Leeds, United Kingdom

*yanko.todorov@ens.fr

Table of content:

1. Sample layout and fabrication

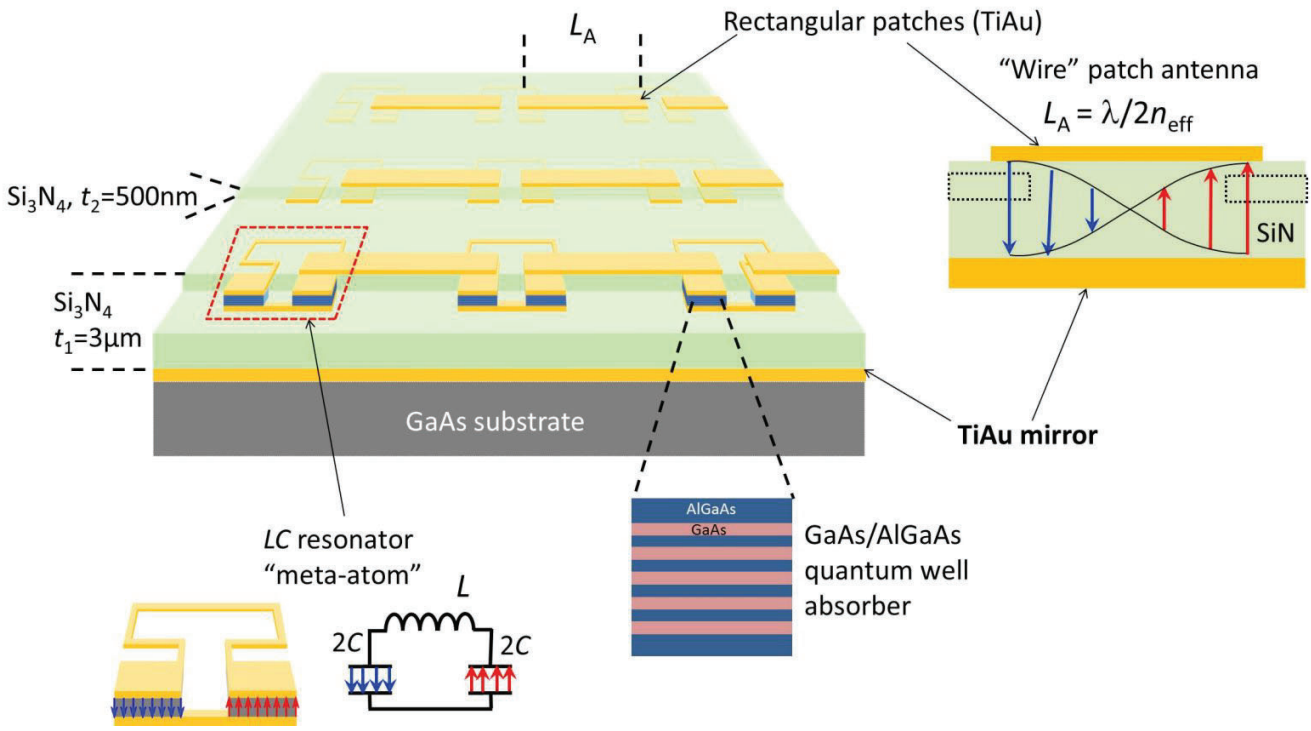

Figure S1: **Full schematics of the structure**. As a result of the fabrication process, the antenna coupled-metamaterial is bonded on a GaAs host substrate through an adhesive (not shown). A planar metallic mirror (Ti: 5 nm, Au: 150 nm) is evaporated on the adhesive+substrate in order to decouple them from the rest of the structure. The LC meta-atoms are encapsulated in a t_1=3µm Si_3N_4 layer that has been evaporated on the top of the TiAu mirror. A schematics of the LC resonator meta-atom is shown (see also Ref. [1]). The two capacitive parts of contain each semiconductor GaAs/AlGaAs quantum well absorbing region which is detailed in the next section. To achieve the antenna layer, the LC meta-material is covered by another t_2= 500 nm thick Si_3N_4 layer, and rectangular TiAu patches are evaporated on the top of this layer. The patches are aligned with the 1µm wide capacitive parts of neighboring LCs. The combination between the bottom TiAu mirror, the Si_3N_4 layer with full thickness t_1+t_2=3.5µm and the metal patch form a double-metal wire antenna (see Ref. [2,3]). The dotted rectangles on the antenna scheme indicate the capacitive parts of two neighboring LC meta-atoms. In both the antenna and LC resonator schematics, the blue and red arrows indicate the electric field of each resonant structure.

The full structure studied in this work is detailed in Figure S1. It consists of antenna-coupled LC "meta-atom" resonators. The LC resonator fabrication has been described in Ref. [1], but we recall here the main steps. The bottom part of the circuit, composed of two capacitor plates and the straight wire, is patterned on top of the absorbing GaAs/AlGaAs region (detailed in the next Section 2) using standard electron beam lithography (EBL) and electron beam evaporation of the Ti/Au structure. The metal acts as a mask for the subsequent inductively coupled plasma reactive ion etching (RIE-ICP) step defining the capacitor pillars. The whole structure is encapsulated in a t_1=3µm thick Si_3N_4 layer deposited using low-temperature plasma enhanced chemical vapor deposition (LT-PECVD) at 150°C, followed by the deposition of a metallic (Ti: 5 nm, Au: 150 nm) mirror. The sample is then bonded to a host GaAs substrate using epoxy glue, and the original growth substrate is etched away, revealing the absorbing region encapsulated in Si_3N_4. The final part of the LC resonator can then be patterned in a

co-aligned fashion using EBL again. As a result of this fabrication process, we obtain an array of three-dimensional LC resonators each with two capacitve parts; the GaAs/AlGaAs absorbing region is placed only in the capacitors, while the rest of the resonators is encapsulated in the t_1=3 μm thick Si_3N_4 layer.

To achieve the antenna layers, we then add a t_2=500nm thick Si_3N_4 layer using LT-PECVD. This layer modifies the dielectric environment of the LC resonator, thus changing its resonant frequency, as discussed in section 7. Finally, the antennas are fabricated using EBL. As shown in Figure S1, the combination between each metal patch, the Si_3N_4-spacer with full thickness t_1+t_2=3.5 μm and the bottom planar TiAu mirror form a patch antenna resonator [2,3], which sustains a fundamental half-wavelength mode with a resonant wavelength $\lambda=2n_{eff}L_A$, where L_A is the length of the metal stripe and n_{eff} an effective index, as commented in the main text. Since the stripe width, 1 μm, is typically much smaller than L_A~10 μm, this type of patch antenna is called "wire patch antenna" [3].

2. Absorbing region design and characterization

The absorbing region hosting the two dimensional electron gas consists in five 32 nm GaAs quantum wells (QWs) separated by 20 nm $Al_{0.15}Ga_{0.85}As$ barriers. In the final device, shown in Fig. S1, absorbing region is sandwiched between the two metal layers of the capacitors of the LC resonators. The QWs are modulation-doped by Si δ-doped regions placed 5 nm away from the QW, with a nominal sheet carrier density of 2×10^{11} cm^{-2}. As detailed in previous work [1], care must be taken in designing the 300 nm thin active region to avoid depletion of the QWs due to the band bending at the metal-semiconductor interfaces. To compensate for this effect, we introduced doped GaAs and $Al_{0.15}Ga_{0.85}As$ layers on each side of the active region.

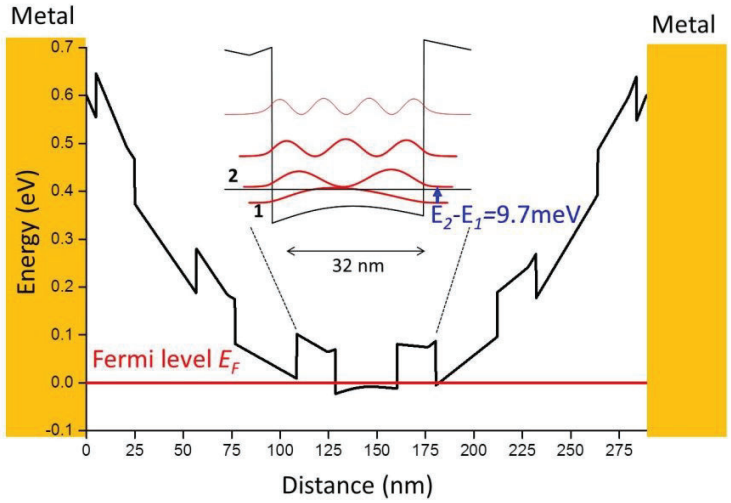

Figure S2: Bandstructure diagram of the absorbing region with 5QW embedded between two metals. Owe to band bending and carrier depletion effects only the central QW is effectively doped and optically active.

In order to fully characterize the active region and determine precisely the relevant parameters for the analysis presented in the main text, we use the same approach as in Refs. [1-3]. We process square patch double metal microcavities on the exact same sample. Such double-metal cavities sustain a resonance at $\lambda=2n_{eff}s$ where s is the size of the patch, and n_{eff} the effective index of the confined mode. They will serve as a reference to our current LC samples [1-3].

Patch cavities and LC resonators without antenna are studied in a reflectivity experiment at low temperature, from which we extract the frequencies of the upper and lower polaritons. Using the procedure detailed in Ref. [1] we determine that the doping layer only moderately compensate for the band bending. In the case of the patch cavities, we find that only a single QW is doped at 1.6×10^{11}cm^{-2} (Figure S2). Lateral depletion in the 1 μm wide semiconductor pillars forming the capacitor are responsible for a lower doping of the QWs in the LC resonator sample, which explains why it shows a slightly lower vacuum Rabi splitting and intersubband plasmon frequency than its patch cavity counterpart. However, we can determine that the doping density is 1.4×10^{11}cm^{-2}, and the effective mode volume is $V_{\text{eff}} = 1.2V_0=10^{-6}\lambda_0^3$, where V_0 =1 μm x 1 μm x 0.3 μm= 0.3μm^3 is the volume of the semiconductor material in each capacitive part and λ_0 is the resonant wavelength of the LC meta-atom.

3. Maximum absorption cross section of a quantum well "particle"

We consider a cubic "particle" filled with the quantum wells described in the main text. The system is a "particle" in the sense that its dimensions are much smaller than the wavelength λ that corresponds to the energy of the electronic transition of the quantum wells. In particular, the absorbing region inserted in the capacitive parts of our system can be considered as a particle, since all of its dimensions V_0 = 1 μm x 1 μm x 0.3 μm are much smaller than the typical wavelength λ = 88 μm of the absorbed THz radiation. Our aim is to determine the maximum absorption cross section of the particle when it is illuminated by a plane wave. To this end, we apply a very general theory of Tretyakov [4], which provides the following expression of the absorbing cross section:

$$\sigma_{abs} = \frac{k}{\varepsilon\varepsilon_0}\frac{\xi'' \sin^2\theta}{\xi'^2 + \left(\xi'' + \frac{k^3}{6\pi\varepsilon\varepsilon_0}\right)^2} \tag{S1}$$

Here $k=n\omega/c$ is the propagation wavevector, and ξ', ξ'' are coefficients related to the real and imaginary part of the inverse polarizability α:

$$\frac{1}{\alpha} = \xi' + i\left(\xi'' + \frac{k^3}{6\pi\varepsilon\varepsilon_0}\right) \tag{S2}$$

The quantity ξ'' thus accounts for the non-radiation loss, while the second term in the parenthesis accounts for the radiation loss of the particle. With respect to Ref. [4] we consider anisotropic absorption where dipoles are excited only along the growth axis of the well, and θ is the angle between the dipoles and the direction of propagation of the incident plane wave. Furthermore, we suppose that the particle is inserted in a homogeneous medium with a refractive index n and a dielectric constant $\varepsilon=n^2$.

In order to determine explicitly the coefficients ξ', ξ'' we consider the absorption quantum efficiency of a quantum well system as described in Ref. [5] (page 11, Eq. (20)):

$$\eta = \frac{N_{QW} n_s e^2}{hcn\varepsilon_0}\omega d_{21}^2 \frac{\gamma}{\gamma^2 + (\omega-\omega_{21})^2} \tag{S3}$$

Here N_{QW} is the number of quantum wells, n_s is the areal electron density per well, e is the electron charge, $\hbar$ is the Plank's constant, d_{21} is the dipole matrix element of the quantum well transition, and γ is the broadening of the electronic transition at a frequency ω_{21}. With respect to Eq. (20) in Ref. [5] we have used the explicit expression of the transition oscillator strength $f_{21} = 2m^*\omega_{21}d_{21}^2/\hbar$, with m^* the effective electron mass.

In order to identify the coefficients ξ', ξ'' from (S3) we proceed as follows. We consider a finite surface of the particle S, then the absorption cross section becomes $\sigma_{abs}=\eta S$. Furthermore, the theory in Ref. [5] is valid for negligible radiation loss, $\xi'' >> k^3/6\pi\varepsilon\varepsilon_0$ and optimum overlap with the impinging electric field, $\sin\theta=1$. Comparing (S1) and $\sigma_{abs}=\eta S$ with these approximations, we obtain the following identifications:

(S4) $$\xi' = \beta(\omega - \omega_{21}),\ \ \xi'' = \beta\gamma$$

(S5) $$\beta^{-1} = \frac{N_{QW}N_e e^2 d_{21}^2}{\mathrm{h}}$$

Here $N_e = n_s S$ is the total number of electrons in each quantum well. Replacing back into (S1), we obtain are very general expression of the absorption cross section of the quantum well particle at resonance $\omega = \omega_{12}$:

(S6) $$\sigma_{abs} = \frac{3\lambda^2}{8\pi\varepsilon\varepsilon_0}\sin^2\theta\frac{4\gamma\Gamma_{rad}}{(\gamma+\Gamma_{rad})^2}$$

Here Γ_{rad} is the emission rate of the particle:

(S7) $$\Gamma_{rad} = n\frac{N_{QW}N_e e^2 d_{21}^2}{6\pi\varepsilon_0 c^3 \mathrm{h}}\omega_{21}^3$$

Here the prefactor $N_{qw}N_e$ expresses the superradiant nature of the quantum well emitter [6]**.** Clearly, equation (S6) is a very general result that can be applied to any solid-state emitter. In accordance with the general result stated in Ref. [4] the maximum possible absorption cross section is $\sigma_{abs} = 3\lambda^2/8\pi\varepsilon$, reached in the case where radiation and non-radiation loss are equal, $\gamma = \Gamma_{rad}$. This condition is very similar to the critical coupling condition for total absorption in quantum well slabs with areas much larger than λ^2 [7].

Using the parameters of our devices, from (S7) we estimate $\Gamma_{rad} = 3.2\text{x}10^{-5}$ THz and Coupled-Mode Theory (CMT) fits provide $\gamma = 0.2$ THz, as explained further. Note that the value of γ compares very well with the typical linewidth of the absorption spectra obtained from very similar quantum well samples [2].

4. Absorption cross section from Coupled-Mode Theory

We now translate the results of the previous section in terms of Coupled-Mode Theory. This formalism allows considering more complex situations where the absorber is coupled to an antenna or to an antenna-coupled microcavity.

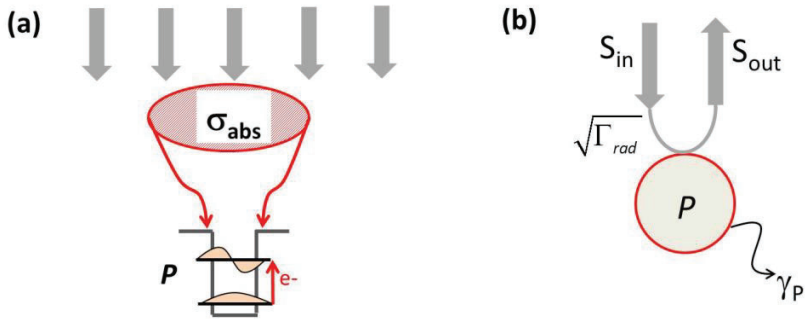

Figure S3. Single absorber coupled to free space. (a) The absorption process can be quantified in terms of an absorption cross section σ_{abs}, defined such as all of the photons impinging on the area σ_{abs} are absorbed by the system. (b) The problem translated in the language of the CMT. An incident photon flux is coupled to the emitter/absorber with a coupling parameter Γ_{rad}. The internal loss rate of the absorber is γ_P.

a) Single absorber coupled to free space.

We consider a single absorber described in terms of a macroscopic polarization vector P coupled with the free space (Fig. S3). In that case the CMT equations become:

$$\frac{dP}{dt} - (i\omega_P - \gamma_P - \Gamma_{rad})P = \sqrt{2\Gamma_{rad}}S_{in} \tag{S8}$$

$$S_{out} = -S_{in} + \sqrt{2\Gamma_{rad}}P \tag{S9}$$

This equation is easily solved in the harmonic regime. Considering the resonant case $\omega = \omega_P$, we can infer the rate of energy absorption $2\gamma_P|P|^2$ normalized on the incident photon flux $|S_{in}|^2$:

$$\eta = \frac{2\gamma_P |P|^2}{|S_{in}|^2} = \frac{4\gamma_P \Gamma_{rad}}{(\gamma_P + \Gamma_{rad})^2} \tag{S10}$$

This quantity provides the fraction of incoming photons that are absorbed by the nano-particle. The function at the right hand side of equation (S10) is always less than unity, and peaks at 1 when $\gamma_P = \Gamma_{rad}$. By comparing with the previous result, (S6), we obtain Eq.(2) in the main text. Note that our theory is developed for the case where only the reflection port is present, but not the transmission; this corresponds to experiments with quantum wells [5], however does not constitute an important restriction of our theory.

In a periodic array with a unit cell area Σ each unit cell receives an incident power $\Sigma|S_{in}|^2$. A fraction η of this power is absorbed by the electronic system with a rate $2\gamma_P$. Since the power absorbed by the electronic system is $\eta\Sigma|S_{in}|^2$ the absorption cross section in a periodic system is $\sigma_{abs} = \eta\Sigma$, as stated by eq. 3 in the main text. This is compatible with the result by Tretyakov [4], except for a factor of 2 as in our case the transmission port is absent.

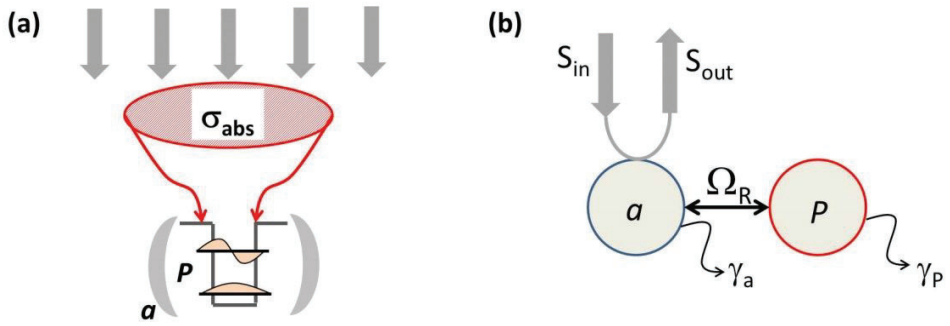

Figure S4 (a) Single absorber *P* coupled to an electromagnetic resonator *a*. (b) The problem translated in the language of the CMT.

b) Absorber coupled to a resonator

We now consider the case where the absorber is inserted in a resonator, as depicted in Figure S4. The resonator is coupled to free space through a radiation loss rate Γ_a. The absorber and the resonator interact with a coupling constant Ω_R. The electromagnetic resonator is characterized by a non-radiative loss rate γ_a and a resonant frequency ω_a. It can be called an "antenna" if its radiation loss is much stronger than the non-radiative one, $\Gamma_a >> \gamma_a$, or a "microcavity" in the opposite regime: $\Gamma_a << \gamma_a$. For simplicity we neglect the possible leakage of photons directly from free space to the absorber, as we suppose that the intrinsic coupling of the absorber to free space is very weak, $\gamma_P >> \Gamma_{rad}$. The CMT equations now become:

(S11) $$\frac{dP}{dt} - (i\omega_P - \gamma_P)P = i\Omega_R a$$

(S12) $$\frac{da}{dt} - (i\omega_a - \gamma_a - \Gamma_a)a - i\Omega_R P = \sqrt{2\Gamma_a}S_{in}$$

(S13) $$S_{out} = -S_{in} + \sqrt{2\Gamma_a}a$$

We now assume that the absorber and the resonator are resonantly coupled, $\omega_a=\omega_P$. Guided by the definition (S10), we look to express the fraction of incident photons effectively absorbed by the polarization *P*, $\eta = 2\gamma_P|P|^2/|S_{in}|^2$, which also provides the absorption cross section in the system.

We now have an additional parameter Ω_R, which allows the system to be in the weak or strong coupling regime. We first examine the frequency dependence of the parameter η for different values of the coupling strength Ω_R. To this end, we use the parameters for the LC resonators as described in the main text. In Figure S5 (a) we plot the ratio η as a function of the frequency for different values of the Rabi frequency. For small values of Ω_R the absorption is maximum at the frequency $\omega=\omega_P=\omega_a$ as expected.

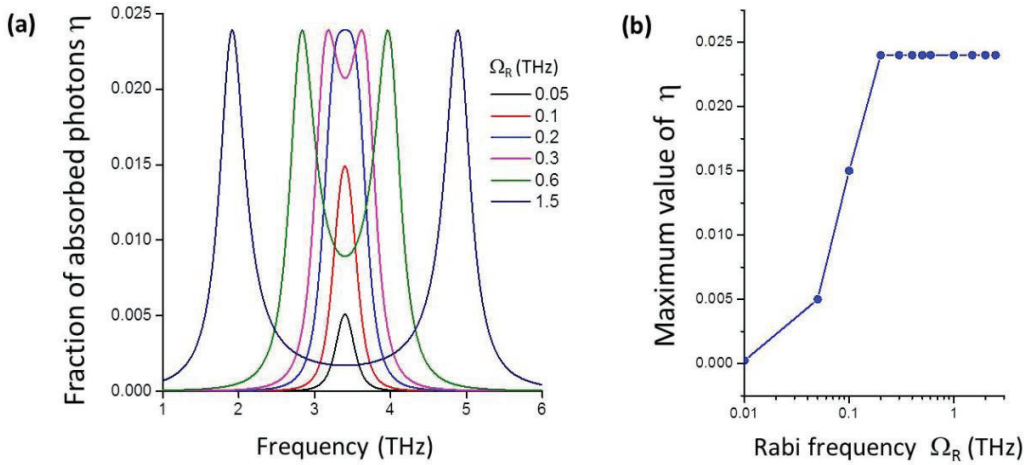

Figure S5. (a) Spectral dependence of η for different values of the coupling constant Ω_R. (b) Peak values of η as a function of the coupling constant Ω_R.

For sufficiently high values of Ω_R the system enters the strong coupling regime, and two eigenstates appear that are mixed light-matter coupled polariton states. The absorption is maximum at the frequencies of the two polariton states, which are provided by:

(S14) $$\omega_{\pm} = \omega_P \pm \Omega_R$$

It is interesting to note that, once the system reaches the strong coupling regime, the peak value of the absorption coefficient η becomes constant. Using equations (S11-S14) we can obtain an expression for the maximum coefficient that is valid both for the weak and strong coupling regimes:

(S15) $$\eta = \frac{4\gamma_P \Omega_R^2 \Gamma_a}{\Omega_R^2(\gamma_P + \gamma_a + \Gamma_a)^2 + \gamma_P^2(\gamma_a + \Gamma_a)^2}$$

In the weak coupling regime ($\Omega_R \to 0$), the first term in the denominator of Eq. (S15) is negligible, and we obtain eq. 4 from the main text:

(S16) $$\eta \approx \frac{4\Omega_R^2 \Gamma_a}{\gamma_P(\gamma_a + \Gamma_a)^2} = \frac{4\Omega_R^2/(\gamma_a + \Gamma_a)}{\gamma_P} \times \frac{\Gamma_a}{\gamma_a + \Gamma_a}$$

Here the quantity $4\Omega_R^2/(\gamma_a + \Gamma_a)$ is the coupling rate between the cavity and the electronic polarization. This equation can be understood as product of two branching ratios: the first one is the probability that a photon is emitted from the electronic transition in the cavity mode, $\left(\left[4\Omega_R^2/(\gamma_a + \Gamma_a)\right]/\gamma_P\right.$, and the second that a photon exits the cavity, $\Gamma_a/(\gamma_a + \Gamma_a)$. The probability of a photon absorption is therefore exactly equal to the probability of a photon emission out of the system. Since by definition $\Omega_R << (\gamma_a + \Gamma_a), \gamma_P$ the absorption efficiency is very small.

In the opposite limit of strong coupling with large Ω_R the second term in the denominator of Eq. (S15) becomes negligible, and we have:

(S17) $$\eta \approx \frac{4\gamma_P \Gamma_a}{(\gamma_P + \gamma_a + \Gamma_a)^2} \approx \frac{4\gamma_P \Gamma_a}{(\gamma_P + \Gamma_a)^2}$$

We have further assumed that $\Gamma_a >> \gamma_a$. This expression is very similar to eq.(S10), expect that now the radiative loss rate of the absorber is replaced with that of the microcavity/antenna. In that case the coupling with the antenna is clearly an advantage, as antennas can be designed as very efficient absorbers/receivers, and the system can be brought close to the ideal limit of almost perfect absorption $\eta \approx 1$. However, this limit implies that the nano-particle is in the strong coupling regime with the optical resonator that acts as an antenna. The coupling constant is inversely proportional to the square root of the effective mode volume, $\Omega_R \approx 1/V_{eff}^{1/2}$. This implies that perfect absorption can be achieved in systems that have both large radiation loss and provide very small effective volumes. This requirement is not naturally satisfied with optical antennas. For instance, in the case of double-metal structures the radiation loss is proportional to the effective volume V_{eff} [3]. We therefore consider a more complex situation as described in the next paragraph.

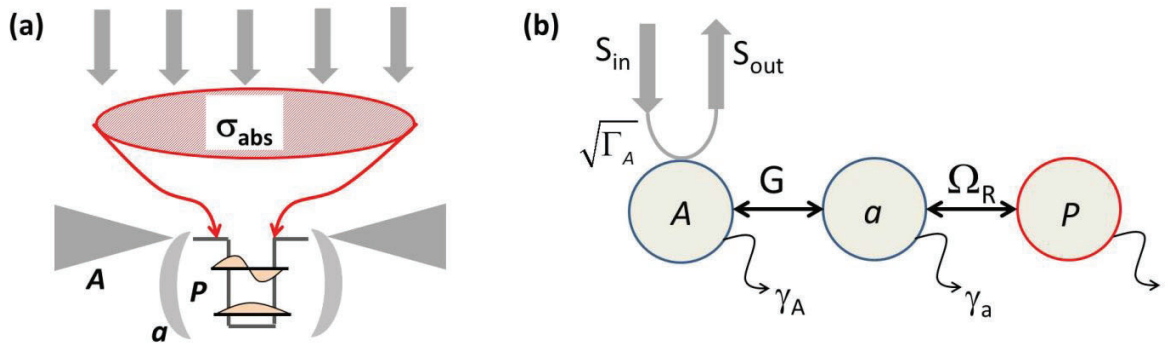

Figure S6. (a) Absorber coupled to an electromagnetic resonator, which is itself coupled to an antenna element. (b) The problem translated in the language of the CMT.

c) Absorber inserted in an antenna-coupled resonator

We now consider a system which can have both a large radiative loss and where the absorber is strongly coupled to an electromagnetic resonator. This situation is depicted in Figure S6. The absorber is coupled to an electromagnetic resonator ("*a*") for which we neglect the radiative loss. The resonator is coupled to an antenna ("*A*") through a coupling constant *G*. In order to simplify our analysis, we neglect the non-radiative loss of the antenna. The CMT system of equations now becomes:

(S18) $$\frac{dP}{dt} - (i\omega_P - \gamma_P)P = i\Omega_R a$$

(S19) $$\frac{da}{dt} - (i\omega_a - \gamma_a)a - i\Omega_R P - iGA = 0$$

(S20) $$\frac{dA}{dt} - (i\omega_A - \Gamma_A)A - iGa = \sqrt{2\Gamma_A}S_{in}$$

(S21) $$S_{out} = -S_{in} + \sqrt{2\Gamma_A} A$$

As for the previous case, we first consider the spectral dependence of the parameter η as a function of the Rabi frequency Ω_R. This is shown in Figure S7, where we have considered that the three oscillators are resonant, $\omega_P = \omega_a = \omega_A$. The parameters for the coupling coefficient G and the loss parameters that we consider are the ones for our systems. In the strong coupling regime, the absorption is maximum at the polariton frequencies, however the absorption remain strong at the central frequency $\omega_P = \omega_a = \omega_A$. Furthermore, the peak absorption now has non-trivial dependence on Ω_R. Therefore, in order to understand our system, it is sufficient to consider the peak absorption at the central frequency $\omega_P = \omega_a = \omega_A$.

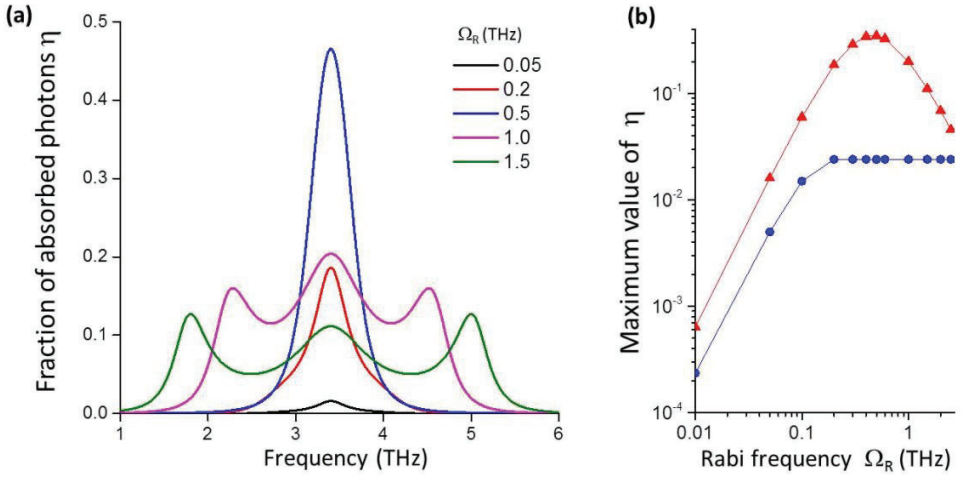

Figure S7. (a) Spectral dependence of η for different values of the coupling constant Ω_R, for the system shown in Figure S6. (b) Peak values of η as a function of the coupling constant Ω_R. The blue dots correspond to the system in Figure S4, and the red triangles to the system depicted in Figure S6.

The peak absorption coefficient now becomes:

(S22) $$\eta = \frac{4\gamma_P \Omega_R^2 G^2 \Gamma_A}{\left[\gamma_P G^2 + \Gamma_A(\gamma_P \gamma_a + \Omega_R^2)\right]^2}$$

Seen as a function of Ω_R this expression has a bell-like shape that is optimized at a particular value of the Rabi frequency provided by:

(S23) $$\Omega_R^2 = \gamma_P \left(\frac{G^2}{\Gamma_A} + \gamma_a \right)$$

The maximal possible absorption efficency then becomes:

(S24) $$\eta = \frac{G^2}{G^2 + \gamma_a \Gamma_A}$$

This is a simple expression that is independent from the intrinsic loss rate of the absorber. Our system thus introduces degrees of freedom that allow optimizing the photon absorption rate in any type of absorbing particle. The strong subwavelength confinement of the LC resonator allows engineering coupling constants high enough so that the optimizing condition (S23) is satisfied.

5. Fitting experimental spectra with Coupled-Mode Theory

a) Full model

To compare CMT with experiments we estimate the reflection coefficient $R(\omega) = |S_{out}|^2/|S_{in}|^2$ which is compared to the experimental reflectivity spectra. The data is modeled with extended set of equations that correspond to the diagram in Figure S8. With respect to the simplified theory presented above, we include the non-radiative loss of the antenna, γ_A, the radiative loss of the resonator Γ_a, as well as light-matter coupling between the antenna and the polarization Ω_A.

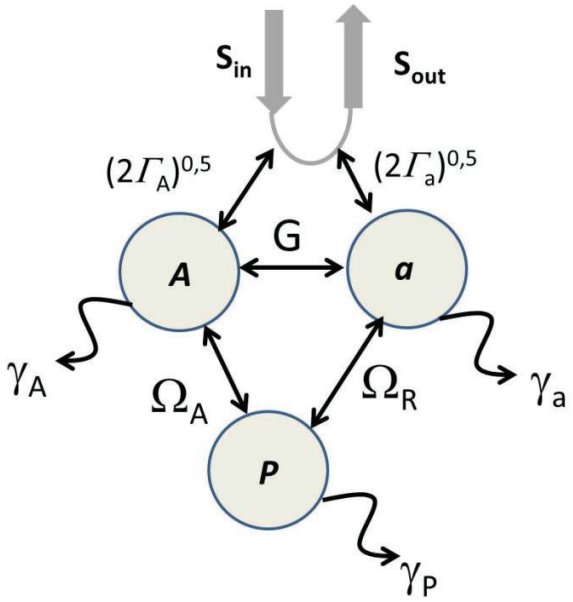

Figure S8. Diagram for the full CMT equations used to model the experimental data.

b) Data and fit parameters for LC structures alone

As stated in the main text, we have studied 4 LC resonators with variable length of the inductor, P_L = 10 µm, 11 µm, 12 µm, 14 µm. An additional structure P_L = 9 µm was fabricated for the optimized antenna-coupled LC as described further. In Figure S9 we present high temperature spectra S9(a), low temperature spectra S9(b) as well as the corresponding η-parameter S9(c). Baseline correction has been applied on the experimental data in order to facilitate the comparison with CMT predictions.

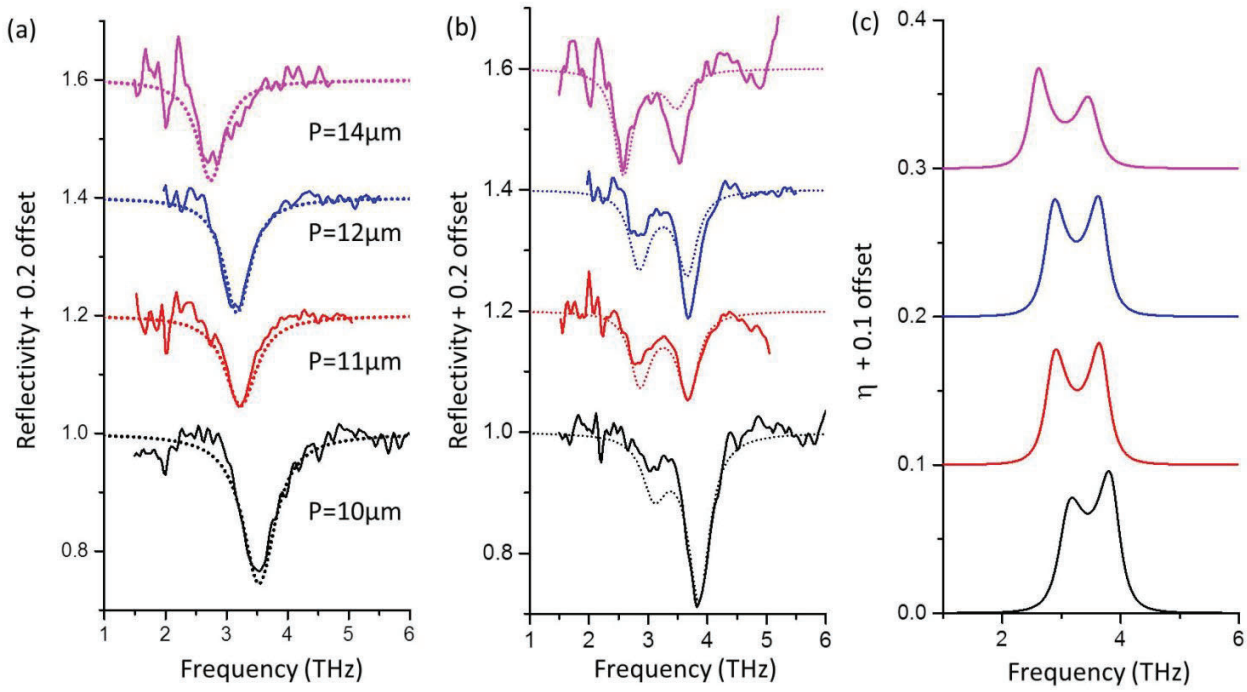

Figure S9. (a) Room temperature spectra of the LC resonators (solid line). The dotted curve is CMT fits. (b) Reflectivity spectra taken with the same samples at 7K. Now the QW is included in the CMT fits. (c) η parameter from CMT.

The following **Table S1** resumes the fit parameters, as well as the value of the array unit cell for each structure:

P_L (μm)	f_{LC} (THz)	γ_a(THz) 300K	γ_a(THz) 7K	Γ_a(THz)	Ω_R(THz)	f_{QW} (THz)	γ_P(THz)	Σ (μm²)
10	3.53	0.3	0.18	0.02	0.4	3.3	0.2	34.8
11	3.23	0.3	0.15	0.0136	0.4	3.3	0.2	39.3
12	3.17	0.25	0.15	0.0136	0.4	3.3	0.2	42.6
14	2.8	0.18	0.15	0.012	0.4	3.3	0.2	51.1

The non-radiation loss increase of the γ_a is due to free carrier absorption [2].

c) Data and fit parameters for antenna-coupled LC, room temperature

In Figure S10 we present the room temperature data for the structures from Figure 4 in the main text. We found that the bare resonances of the antenna-coupled *LC* had a systematic shift of -0.3 THz with respect to the *LC* resonator alone, due to the 500nm thick Si_3N_4 covering layer in the antenna geometry (see sections 1 and 8 for details). Therefore we fabricated and additional *LC* structure with P_L=9 μm so that it is resonant with the electronic transition of the quantum well in the antenna-coupled arrays. For that structure we systematically varied the antenna length L_A to explore structures with different antenna resonances f_A.

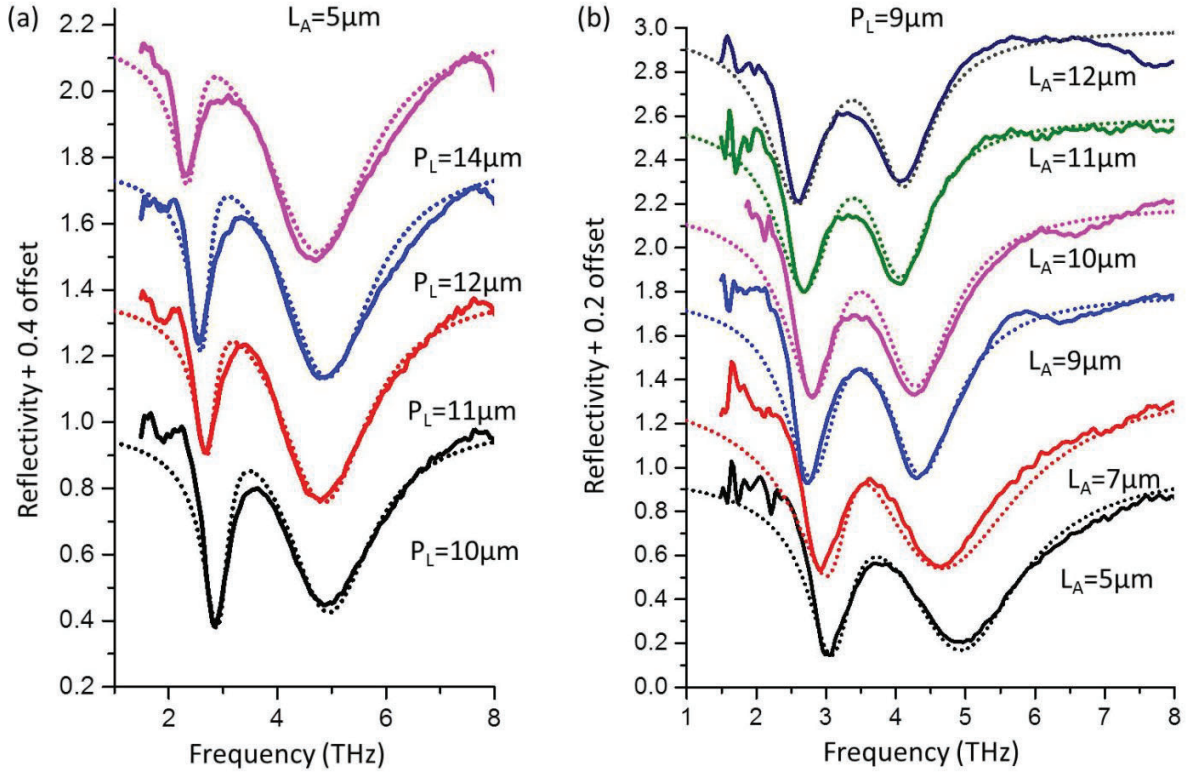

Figure S10. Room temperature spectra of antenna-coupled LC resonators (solid line) with CMT fits (dotted curve). (a) Variable LC resonance (b) Variable antenna resonance.

The following **Table S2** resumes the fit parameters, as well as Σ for each structure:

P_L (µm)	L_A (µm)	f_{LC} (THz)	γ_a(THz) 300K	Γ_a(THz)	f_A (THz)	γ_A(THz) 300K	Γ_A(THz)	G (THz)	Σ (µm²)
10	5	3.18	0.15	0.004	4.65	0.85	0.6	-0.65	34.8
11	5	2.9	0.12	0.00125	4.65	0.85	0.65	-0.6	39.3
12	5	2.85	0.11	0.00125	4.65	0.85	0.62	-0.6	42.6
14	5	2.6	0.16	0.00045	4.65	0.85	0.72	-0.7	51.1
9	5	3.35	0.25	0.011	4.65	0.75	0.75	-0.65	31.8
9	7	3.35	0.2	0.005	4.3	1	0.55	-0.65	42.4
9	9	3.35	0.2	0.0018	3.88	0.48	0.30	-0.75	53
9	10	3.35	0.25	0.0025	3.75	0.6	0.28	-0.65	58.3
9	11	3.35	0.28	0.00045	3.4	0.45	0.245	-0.7	63.6
9	12	3.35	0.28	0.0005	3.35	0.45	0.211	-0.75	68.9

The reduction of γ_A can be explained with reduced Si_3N_4 loss at lower frequencies.

The variations of the coupling parameters Γ_A can also be due to slight misalignments of the setup form one structure to another; this result in variations of the values of the reflectivity dips of the experimental curves. We estimate typical errors to be on the order of 5%.

d) Data and fit parameters for antenna-coupled LC, 7K

The experimental data and fits are presented in Figure 4 of the main text. With respect to the values of Table S2 we observe reduction of the non-radiation loss of the LC and resonances, γ_a =0.15 THz. In the following **Table S3** we provide the evolution of Ω_R in the fits:

P_L (μm)	L_A (μm)	Ω_R(THz)
10-14	5	0.4
9	7	0.4
9	9	0.32
9	10	0.4
9	11	0.38
9	12	0.36

The variations of Ω_R can also be ascribed in temperature variations of the samples.

All other fit parameters are identical or very close to Table S2. Best fits are obtained when we include small QW-antenna coupling Ω_A=0.1 THz, which yields a blue shift of the high energy reflectivity dip at low temperature.

6. Energy conservation from Coupled-Mode Theory

Starting from the CMT equations detailed in the previous paragraph, it is straightforward to obtain the following conservation law:

(S25) $$2\gamma_P |P|^2 + 2\gamma_A |A|^2 + 2\gamma_a |a|^2 = |S_{in}|^2 - |S_{out}|^2 + 4\sqrt{\Gamma_a \Gamma_A}\,\mathrm{Re}(Aa^*)$$

This equation has a clear meaning as it expresses the energy conservation in the system. The terms of the left hand side are easy to interpret as the non-radiative loss rate of the material polarization ($2\gamma_P|P|^2$), the antenna ($2\gamma_A|A|^2$), and of the LC meta-atom ($2\gamma_a|a|^2$). On the right hand side of Eq. (S25) we see the difference between the incoming and out-coming photon flux, $|S_{in}|^2$-$|S_{out}|^2$, a quantity which readily related to the reflectivity of the system $R = |S_{out}/S_{in}|^2$. The last term appears as interference effect between the radiation loss rates of the antenna and the LC resonator. This term is interesting, however it plays little role in the present study because of the assumption that the LC radiation rate Γ_a is small, and shall not be commented further.

So far, we have been exclusively concerned with the fraction of photons $\eta = 2\gamma_P|P|^2/|S_{in}|^2$ absorbed by the material system. However, we can also define quantities $\eta_A = 2\gamma_A|A|^2/|S_{in}|^2$ and $\eta_a = 2\gamma_a|a^2/|S_{in}|^2$ that represent the photons absorbed by the antenna element and the LC resonator; this absorption occur mainly in the metal parts of the electromagnetic resonators, as well as in the Si_3N_4 layer in the case of the antenna. CMT allows discriminating between all types of loss in our complex system. To illustrate this fact and to underline the difference between η which describes the QW absorption only with respect to the other type of losses, we have plotted in Figure S11 the different contributions of eq. (S25). For this plot, we use the CMT parameters that describe low temperature spectrum of the P_L=10 µm L_A=5 µm structure (lowest spectrum in Figure 4(a) from the main text). For this plot we set $|S_{in}|^2 = 1$.

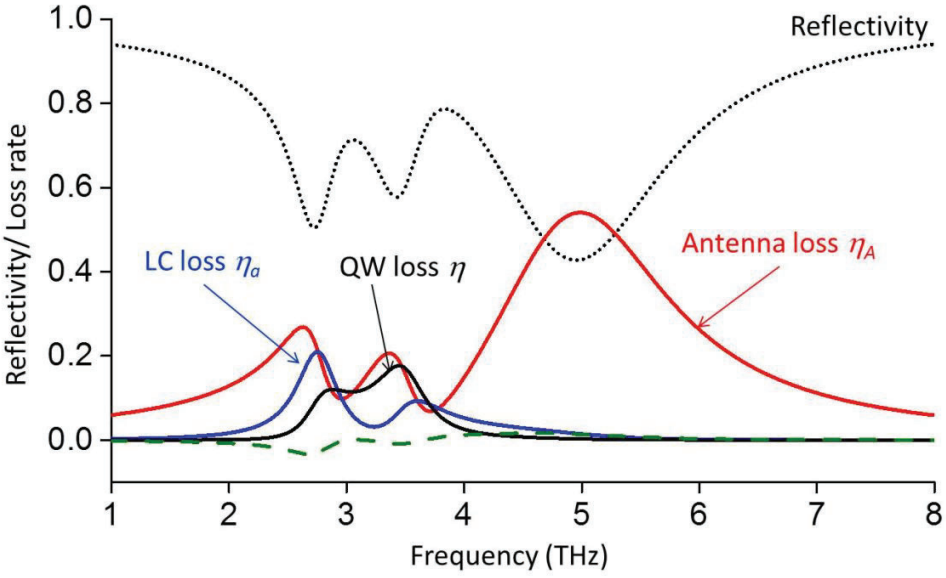

Figure S11: Plots of the different terms of Eq. (S25) using the definitions $\eta = 2\gamma_P|P|^2/|S_{in}|^2$, $\eta_A = 2\gamma_A|A|^2/|S_{in}|^2$ and $\eta_a = 2\gamma_a|a^2/|S_{in}|^2$ for a P_L=10 µm L_A=5 µm structure. The dashed curve represents the interference term (last term in Eq. (S25)).

This plot reveals several interesting features. First, the QW loss appears in a relatively narrow band around the QW electronic transitions. Instead, the antenna loss appears on a very wide frequency range, and it is comparable with the QW absorption even if the antenna resonance is strongly detuned from the electronic transition. We interpret this with the fact that the coupling strength G is very large, and distributes spectrally the antenna loss even at frequencies that are far from the antenna resonance.

7. Finite elements method simulations

While providing a better physical insight on the physics at play in our triply coupled system, the CMT formalism suffers from a large number of free parameters. In order to validate our approach, we carried out finite elements method (FEM) simulations of our system, where the intersubband polarization is modeled through an anisotropic, dispersive complex dielectric permittivity tensor [8,9]. The results are presented in **Error! Reference source not found.,** where we can see that the overall agreement is good. Even though FEM simulations predict resonances with a better quality factor, the frequencies of the coupled resonances are well reproduced. The two approaches thus

give consistent results, but the CMT theory formalism conveniently allows one to deduce the vacuum Rabi splitting as well as other fundamental quantities, such as the absorption cross section as discussed in the main text.

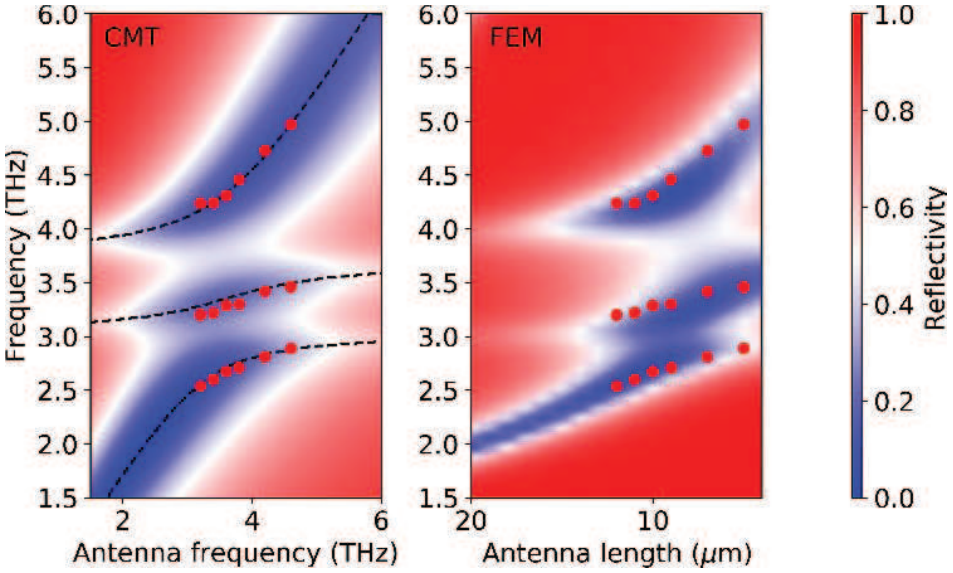

Figure S12: Comparison between the CMT fits (left) and the FEM simulations (right) of the triply coupled system at low temperature. The colormap represents the reflectivity, while the red dots are the experimental data.

8. Effect of the Si_3N_4 coating layer

In order to account for the frequency shift of the *LC* resonance induced by 500nm Si_3N_4 layer (see Figure S1) we performed finite element method simulations of the response of a LC resonator in the presence and absence of this layer. A typical simulation result is shown in Figure S13. The *LC* resonance is the lowest frequency one, which experiences a red-shift of around 0.4 THz in the presence of the Si_3N_4 cover. This value is close to the one used in our CMT fits of the room-temperature spectra of the *LC* resonators before and after antenna fabrication (~0.3-0.4 THz).

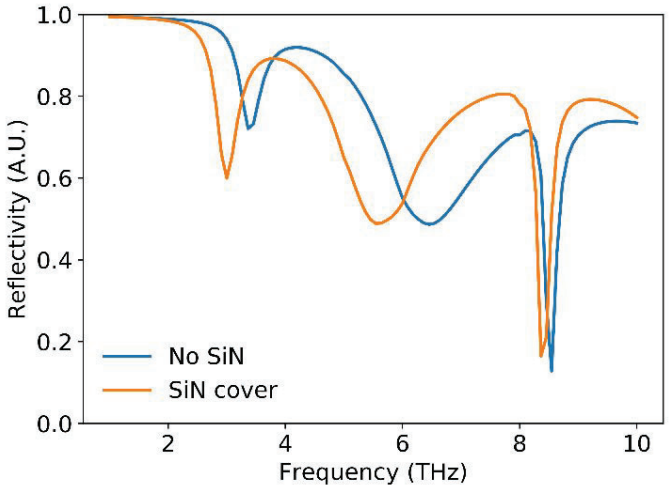

Figure S13: Effect of the 500 nm thick Si_3N_4 layer on the reflectivity spectrum of the LC resonator array.

9. Temperature dependence of the reflectivity spectra

For completeness we provide in Figure S14 typical examples of the reflectivity spectra as a function of the temperature, without any baseline corrections.

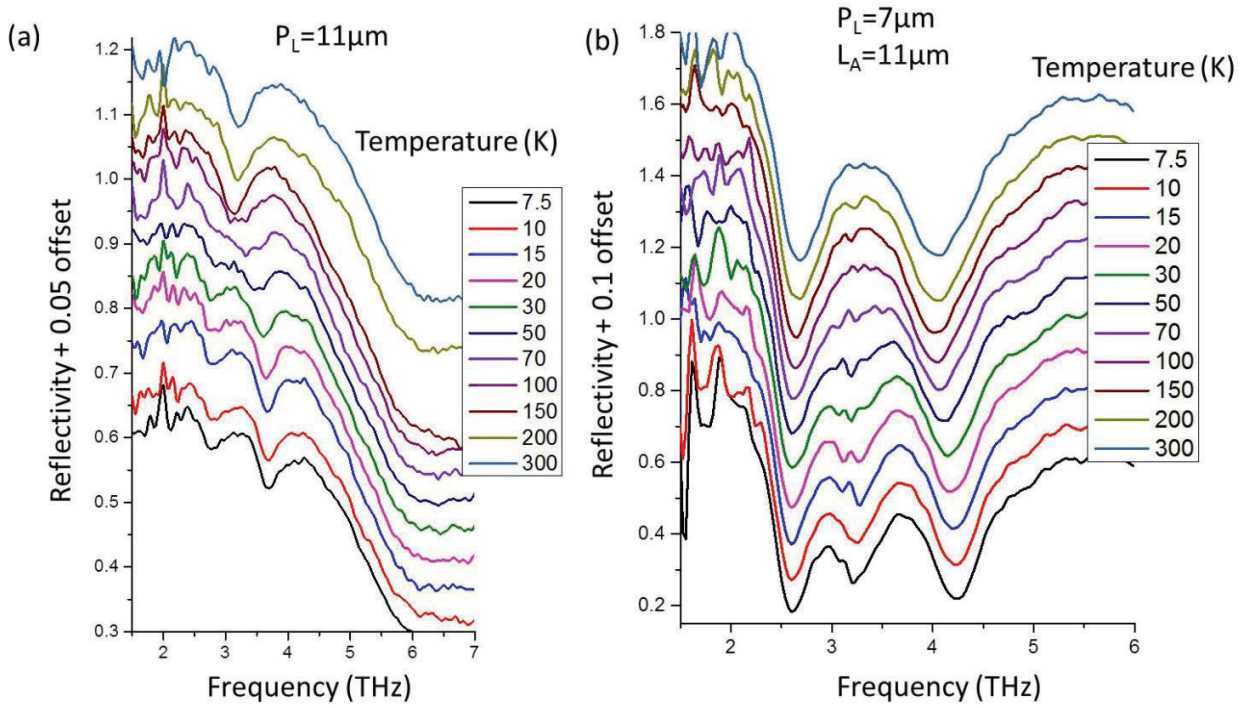

Figure S14: Temperature evolution of the reflectivity spectra, in the case of (a) LC resonator, (b) Antenna-coupled LC resonator. As the temperature is decreased, one can observe the appearance of the absorption feature related to the QW.

References

[1] M. Jeannin *et al.*, ACS Photonics, **6**, p. 1207, (2019)
[2] Y. Todorov *et al.*, Phys. Rev. B, **86**, p. 125314, (2012).
[3] C. Feuillet-Palma *et al.*, Opt. Express, 20, p. 29121, (2012).
[4] S. Tretyakov, Plasmonics, **9**, p. 935-944, (2014).
[5] M. Helm, Academic press, San Diego, 2000.
[6]T. Laurent *et al.*, Appl. Phys. Lett., **107**, p. 241112, (2015).
[7] S. Huppert *et al.*, Phys. Rev. B, **94**, (2016).
[8] R. J. Warburton *et al.*, Phys. Rev. B, **53**, p. 7903-7910, (1996).
[9] T. Ando, A. B. Fowler, et F. Stern, Rev. Mod. Phys., **54**, p. 437-672, (1982).